Geological Survey of Norway
NO-7441 Trondheim, Norway

REPORT

Report no.: 2005.83 | ISSN 0800-3416 | Grading: Open

Title: Permanent Scatterer InSAR processing: Forsmark

Authors: Dehls, J. F.

Client: Svensk Kärnbränslehantering AB

County:

Commune:

Map-sheet name (M=1:250.000)

Map-sheet no. and -name (M=1:50.000)

Deposit name and grid-reference:

Number of pages: 28 Price (NOK): 650

Map enclosures: 3

Fieldwork carried out:	Date of report:	Project no.:	Person responsible:
	15.02.2006	2961.06	Jan S. Rønning

Summary:

It has been speculated that slow, aseismic movement may be occurring along some of the fracture zones crosscutting the Forsmark area. The purpose of this study is to determine if it is possible to measure such movement using dInSAR.

Differential SAR Interferometry (DInSAR) is a technique that compares the phases of multiple radar images of an area to measure surface change. The method has the potential to detect millimetric surface deformation along the sensor – target line-of-sight. Differences in phase between two images are easily viewed by combining, or interfering, the two phase-images. In the resulting image, the waves will either reinforce or cancel one another, depending upon the relative phases. The resulting image is called an interferogram and contains concentric bands of colour, or fringes, that are related to topography and/or surface deformation. New algorithms use many images acquired over a long time period to determine the movement history of individual objects, refered to as permanent scatterers.

In the current project, standard PSInSAR processing was performed on 40 ERS-1 and ERS-2 scenes by Tele-Rilevamento Europa (a POLIMI spin-off company). The total area processed is approximately 1500 km2. Slightly less than 20 000 permanent scatterers were identified.The highest densities were obtained along the coast and on the islands, where natural outcrops are more abundant.

Two main classes of objects act as permanent scatterers in this area. The first are natural reflectors, such as rocks. The second are man-made reflectors, such as parts of buildings. Numerous local movements were found in the study area, relating to building subsidence, or compaction of anthropogenic fill.

The dataset was divided into three groups for analysis, based upon the location of regional lineaments provided by SKB. Both statistical and geostatistical techniques were used. The median velocity of the three blocks did not differ by more than 0.2 mm/yr. This is not considered significant, given the possible magnitude of errors. Surfaces fitted to the three datasets did not reveal any significant spatial patterns related to the fracture zones.

Analysis of movement trends across regional lineaments does not support the hypothesis of slow, aseismic vertical movement taking place along these features. Horizontal movement cannot be ruled out.

For future monitoring applications, it would be useful to install artificial reflectors in well-chosen locations. It would be advantageous if SKB arranged for the acquisition of both ENVISAT and Radarsat images over possible monitoring sites on a regular basis for future analysis.

Keywords:	Interferometry	Subsidence

CONTENTS

FIGURES

MAPS

Mapsheet 2005.083-01. Average relative velocity, 1992-1000, from differential radar interferometry. Forsmark. 1:20,000

Mapsheet 2005.083-02. Average relative velocity, 1992-1000, from differential radar interferometry. Forsmark. 1:50,000

Mapsheet 2005.083-03. Vertical standard deviation of average relative velocity, 1992-1000, from differential radar interferometry. Forsmark. 1:50,000

1. Introduction

Detection and measurement of ground movements has traditionally been the job of surveyors and geodesists. Techniques have included surveying using traditional sights and rods, surveying using new laser tools, and recently high precision GPS instruments. The use of GPS networks has good potential, but has several drawbacks; vertical movements are resolved less accurately than horizontal movements, the stations must be either permanently occupied or at least occupied for several days each year, and there are practical and financial limits as to how many stations can be set up for a given area. In the last decade a new technique using radar images has been developed, with new applications of the technique being discovered each year. This technique, called differential radar interferometry (dInSAR) is able to resolve millimetre-scale vertical deformation, and promises to be of great use in a number of geological applications. Ideally, the two techniques should be used together to resolve both vertical and horizontal movements.

Numerous topographic and/or geophysical lineaments crosscut the Forsmark area (Isaksson et al., 2004). Several of the largest of these have been interpreted as fracture zones (SKB, 2004). Recent studies have ruled out likelihood of major late- or postglacial movement on these faults (Lagerbäck et al., 2005). However, it has been speculated that slow, aseismic movement may be occurring along some of these faults due to the isostatic uplift that is taking place. The purpose of this study is to determine if it is possible to measure such movement using dInSAR.

2. Differential SAR Interferometry (dInSAR)

Differential SAR Interferometry (DInSAR) is a technique that compares the phases of multiple radar images of an area to measure surface change. It first became well known after an image of the Landers Earthquake deformation field was published in the journal Nature in 1993 (Massonnett et al., 1993). The method has the potential to detect millimetric surface deformation along the sensor – target line-of-sight.

A radar satellite emits pulses of radar energy, which are scattered by the Earth's surface. When such a pulse of radar energy is reflected back to the satellite, two types of information are recorded. The first information recorded is the amplitude of the signal. This is the information displayed in typical SAR images (Figure 1). The amplitude is influenced by factors such as the surface material, the slope of the surface and surface moisture content.

Figure 1. *SAR image showing Ranafjorden and Svartisen glacier, July 1995.*

The second information recorded is the phase of the wave. ERS satellites have a radar wavelength of 5.66 cm. The phase of the wave upon return depends primarily on the distance between the satellite and the surface. It is also affected by changes in the atmosphere, but this is a very small effect.

Differences in phase between two images are easily viewed by combining, or interfering, the two phase-images. In the resulting image, the waves will either reinforce or cancel one another, depending upon the relative phases. The resulting image is called an interferogram and contains concentric bands of colour, or fringes, that are related to topography and/or surface deformation.

If two images are acquired from different positions within a small period of time, the difference in phase can be used to determine the surface topography (Figure 2). If two images are acquired of the same area from the exact same position, any difference in phase is due to movements of the ground surface toward or away from the satellite during the time between the two images (Figure 3).

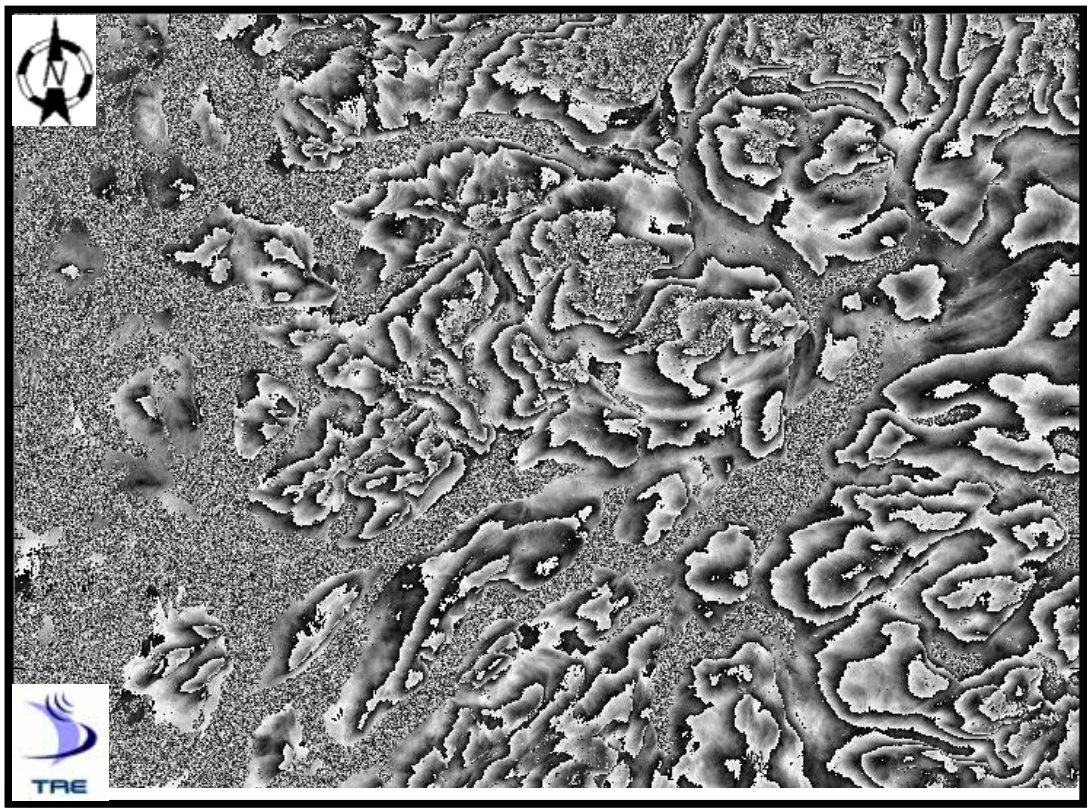

Figure 2. *SAR interferograms obtained from a pair of images acquired July 15 and 16, 1995, by the ERS-1 and ERS-2 satellites. The area is the same as Figure 1. Fringes are related to topography.*

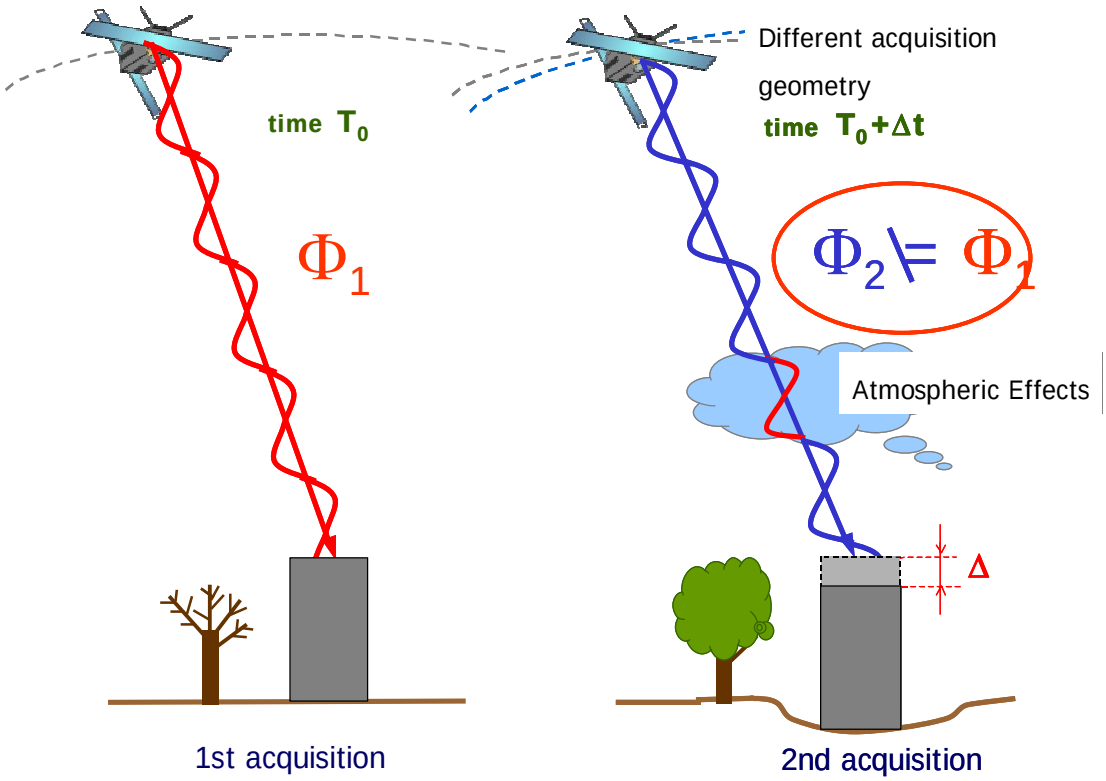

Figure 3. *If two radar images are acquired at different times ftom the same place, differential movement will result in a different measured phase.*

Since it is nearly impossible to obtain two images of the same area from exactly the same point at two different times, three images are typically used to analyse surface change. First, an image pair taken during a short interval is used to determine the topography. Second, an interferogram is created using two images with a longer time interval. The effects of topography are removed using the results of the first interferogram, and the resulting image contains fringes due to surface deformation. Each fringe represents one-half wavelength of surface movement. In the case of the ERS satellites, this is less than 3 cm.

Radar interferometry has one stringent condition that must be met in order for it to work. The many small reflective objects contributing to each pixel must remain unchanged, or *coherent*, between images. Decorrelation may occur due to variations in the complex reflectivity of individual sampling cells as a function of the acquisition geometry (geometric decorrelation) and/or time (temporal decorrelation). In addition, atmospheric phase screen, mainly due to the effect of the local water vapour content, can be difficult to discriminate from ground deformation.

2.1 Permanent Scatterers Technique (PSInSAR)

The SAR processing group at Politecnico di Milano has developed a new method based upon the identification of stable natural reflectors (called permanent scatterers) that are coherent over a long period of time (Ferretti et al., 2001). These permanent scatters (PS) can be identified and used in many images over a long period of time. These scatterers are objects that reflect energy in a wide range of directions so that they are visible to the satellite despite variations in orbit. Typical objects are corners of constructions, vertical structures such as fence posts, and natural reflectors such as sharp rocks or ledges in outcrops.

The PS approach is a two-step processing technique aimed at isolating the different phase terms (atmospheric phase screen, deformation and residual topography) on a sparse grid of phase stable, point-wise radar targets. The PS approach is based on the exploitation of long time-series of interferometric SAR data (at least 25-30 images). The technique is able to overcome both main limiting factors: PS are only slightly affected by decorrelation and can be used to estimate and remove the atmospheric phase screen.

The sparse PS grid can be thought of as a high spatial density (up to 400 PS/km^2, in highly urbanized areas) geodetic network allowing ground deformation measurements (along the line-of-sight direction) with millimetric accuracy (0.1-1 mm/yr on the average line-of-sight deformation rate and 1-3.5 mm on single measures).

Since Permanent Scatterers mainly correspond to portions of man-made structures, and a minimum PS density is required to guarantee the measurements reliability, most significant PS results have been obtained analyzing urban areas and their immediate neighbourhood. The PS approach allows the identification of isolated phase-stable targets in low coherence areas. These provide precise surface deformation data in areas where a conventional dInSAR approach fails due to decorrelation noise.

Since 2001, several other research groups around the world have developed techniques to extract deformation information from a large set of SAR images. While the algorithms differ, they all promise mm-scale accuracy in deformation detection.

2.1.1 Notes about velocity values

Several points must be kept in mind when interpreting the velocity values obtained by this method.

- All values are relative to an arbitrarily chosen reference point that is assumed to be stable.

- In general, the standard deviation of velocity errors increases with distance from the reference point, although there are other contributing factors as well. For this reason, the reference point is chosen as close as possible to the centre of the area of interest (Figure 4 and Mapsheet 3).

- As stated earlier, the velocity given is the velocity along the line-of-sight to the satellite, which is on average 23º from the vertical. If the true movement direction is vertical, the line-of-sight velocity is an underestimate of the true velocity.

- No images are available for 1994 and early 1995. During that year, the European Space Agency used the ERS-1 satellite for several different missions that had a different orbital geometry.

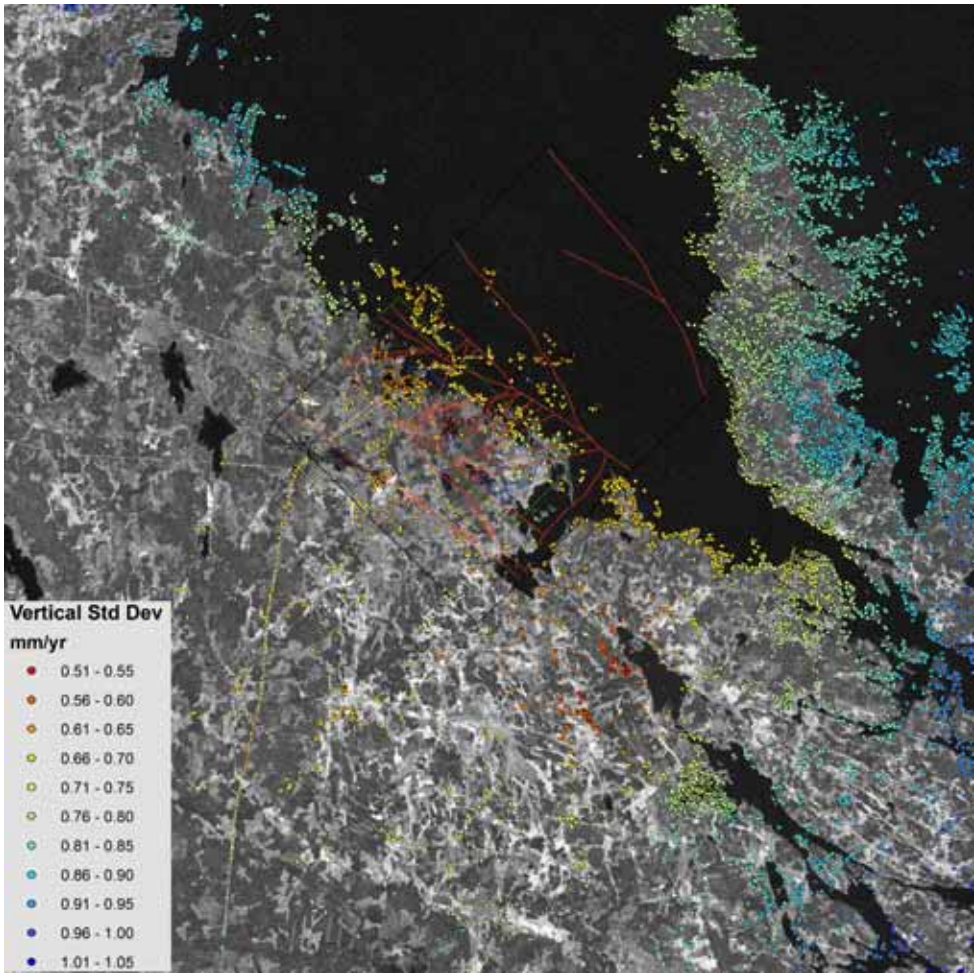

Figure 4. *Vertical standard deviation increased with distance from the reference point. For this reason, the reference point is usually chosen near the centre of the study area.*

3. Overview of Results

In the current project, standard PSInSAR processing was performed on 40 ERS-1 and ERS-2 scenes by Tele-Rilevamento Europa (a POLIMI spin-off company). A further eight scenes acquired after 1999 be discarded to be discarded due to high Doppler centroid values.

Table 1. *List of ERS scenes used in this project.*

#	Acquisition date	Satellite	#	Acquisition date	Satellite
1	8/23/1992	ERS-1	21	6/11/1996	ERS-1
2	11/1/1992	ERS-1	22	6/12/1996	ERS-2
3	1/10/1993	ERS-1	23	7/16/1996	ERS-1
4	2/14/1993	ERS-1	24	12/4/1996	ERS-2
5	3/21/1993	ERS-1	25	1/8/1997	ERS-2
6	5/30/1993	ERS-1	26	2/12/1997	ERS-2
7	8/8/1993	ERS-1	27	3/19/1997	ERS-2
8	10/17/1993	ERS-1	28	4/23/1997	ERS-2
9	4/18/1995	ERS-1	(reference) 29	5/28/1997	ERS-2
10	5/23/1995	ERS-1	30	7/2/1997	ERS-2
11	5/24/1995	ERS-2	31	10/15/1997	ERS-2
12	6/27/1995	ERS-1	32	11/19/1997	ERS-2
13	6/28/1995	ERS-2	33	1/28/1998	ERS-2
14	10/10/1995	ERS-1	34	4/8/1998	ERS-2
15	2/27/1996	ERS-1	35	7/22/1998	ERS-2
16	2/28/1996	ERS-2	36	8/26/1998	ERS-2
17	4/2/1996	ERS-1	37	9/30/1998	ERS-2
18	4/3/1996	ERS-2	38	7/7/1999	ERS-2
19	5/7/1996	ERS-1	39	10/20/1999	ERS-2
20	5/8/1996	ERS-2	40	11/24/1999	ERS-2

The areas of interest specified by the client are shown in Figure 5. In order to get a better understanding of regional trends, a larger area was processed. The total area processed is approximately 1500 km^2. Slightly less than 20 000 permanent scatterers were identified. Since a significant portion of the area is water, the real data density is estimated to be between 15 and 20 PS/km^2. This low density is not surprising considering the rural nature of the area, with much vegetation and few man-made structures. The highest densities were obtained along the coast and on the islands, where natural outcrops are more abundant.

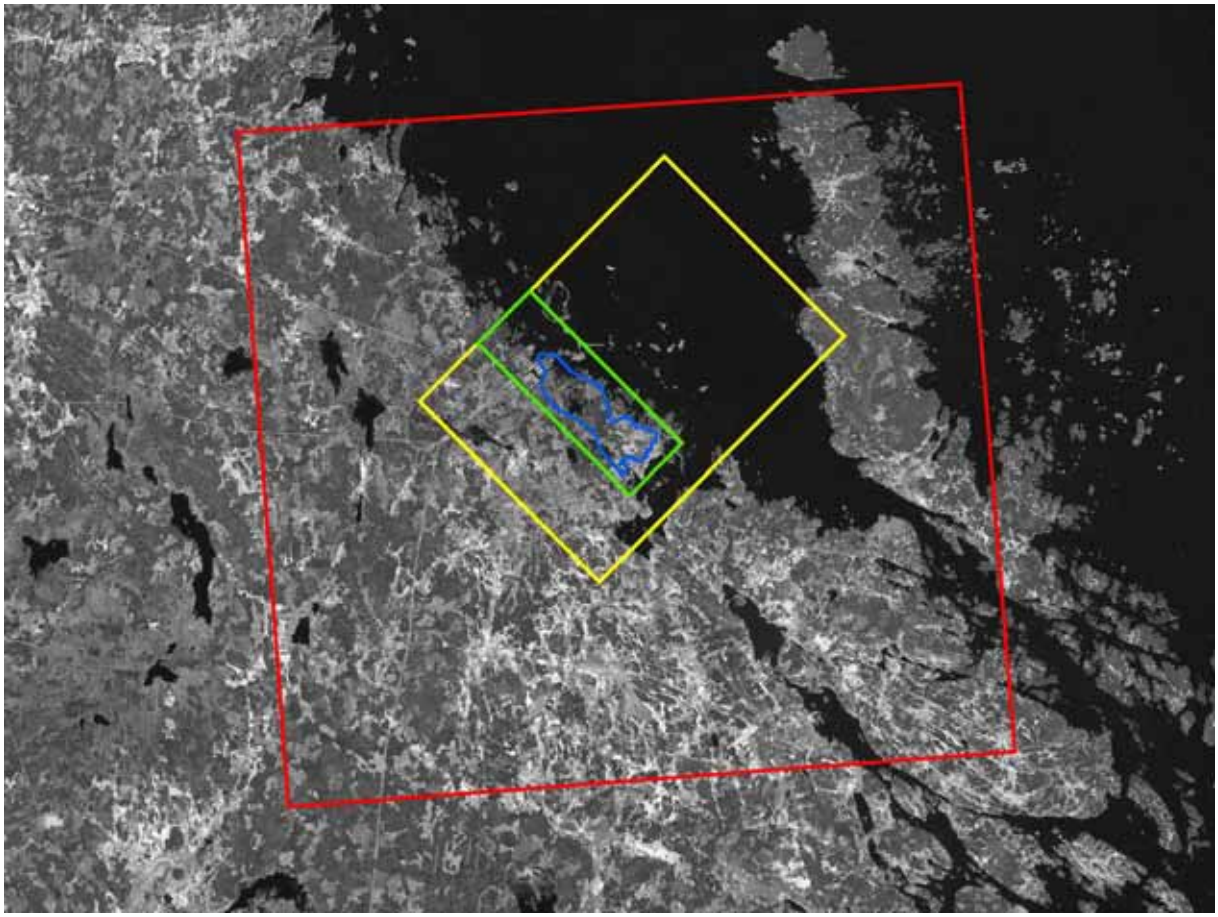

Figure 5. *The candidate area is marked in blue. The green rectangle is the local model area. The yellow rectangle is the regional model area. The area marked in red is the area for which PSInSAR processing was carried out.*

3.1 Types of deformation seen

Mapsheet 1 shows the PS around the site area, at a scale of 1:20,000. Figure 6 shows the deformation seen around the power plant. While the buildings themselves are stable, there are a number of data points that show subsidence. Most of these are in areas of fill along the waterfront. The deformation rate is constant, as shown by the displacement vs. time graph shown in Figure 7.

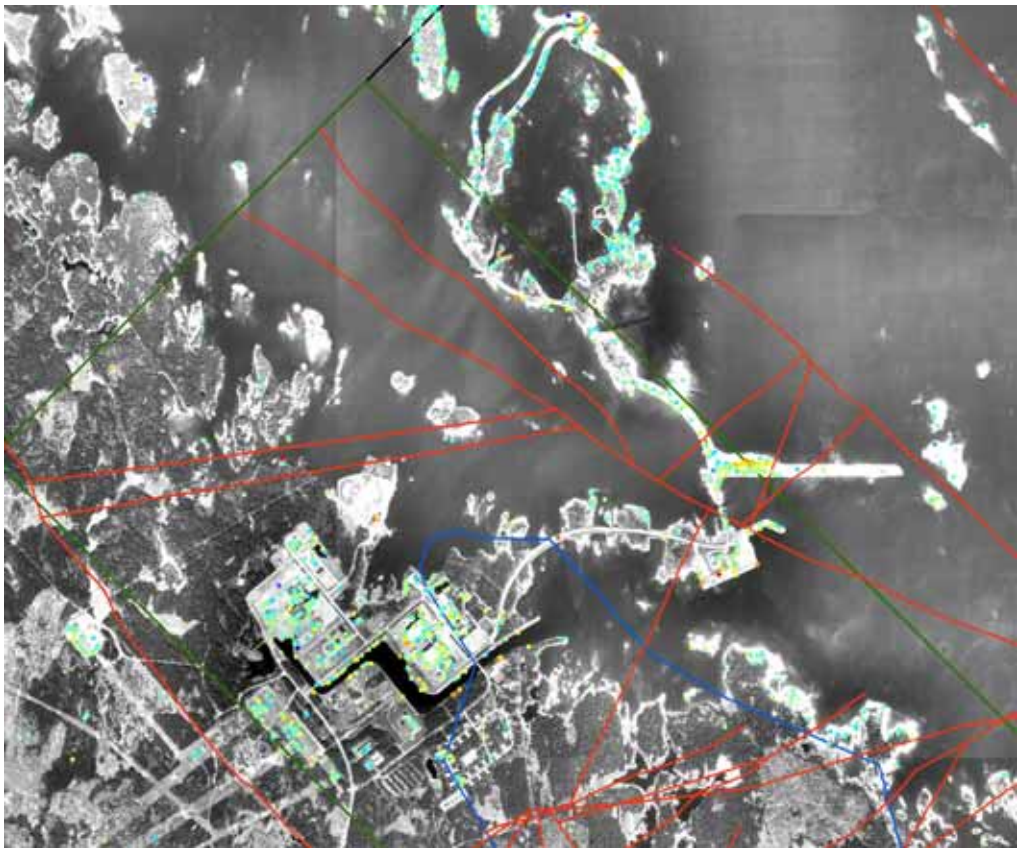

Figure 6. *Extract from Mapsheet 1, showing deformation around the power plant.*

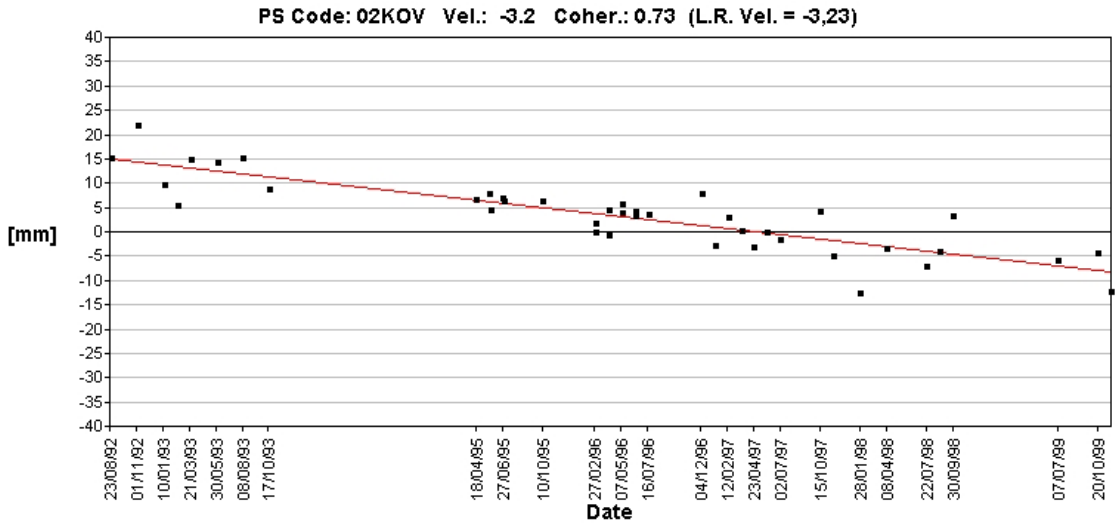

Figure 7. *Displacement vs. time for one of the points on the pier behind the SKB building at Forsmark.*

Figure 8 is also taken from Mapsheet 1, slightly southwest of Figure 6. Vertical metal structures, such as those along the power line, are exceptionally good scatterers, almost always visible.

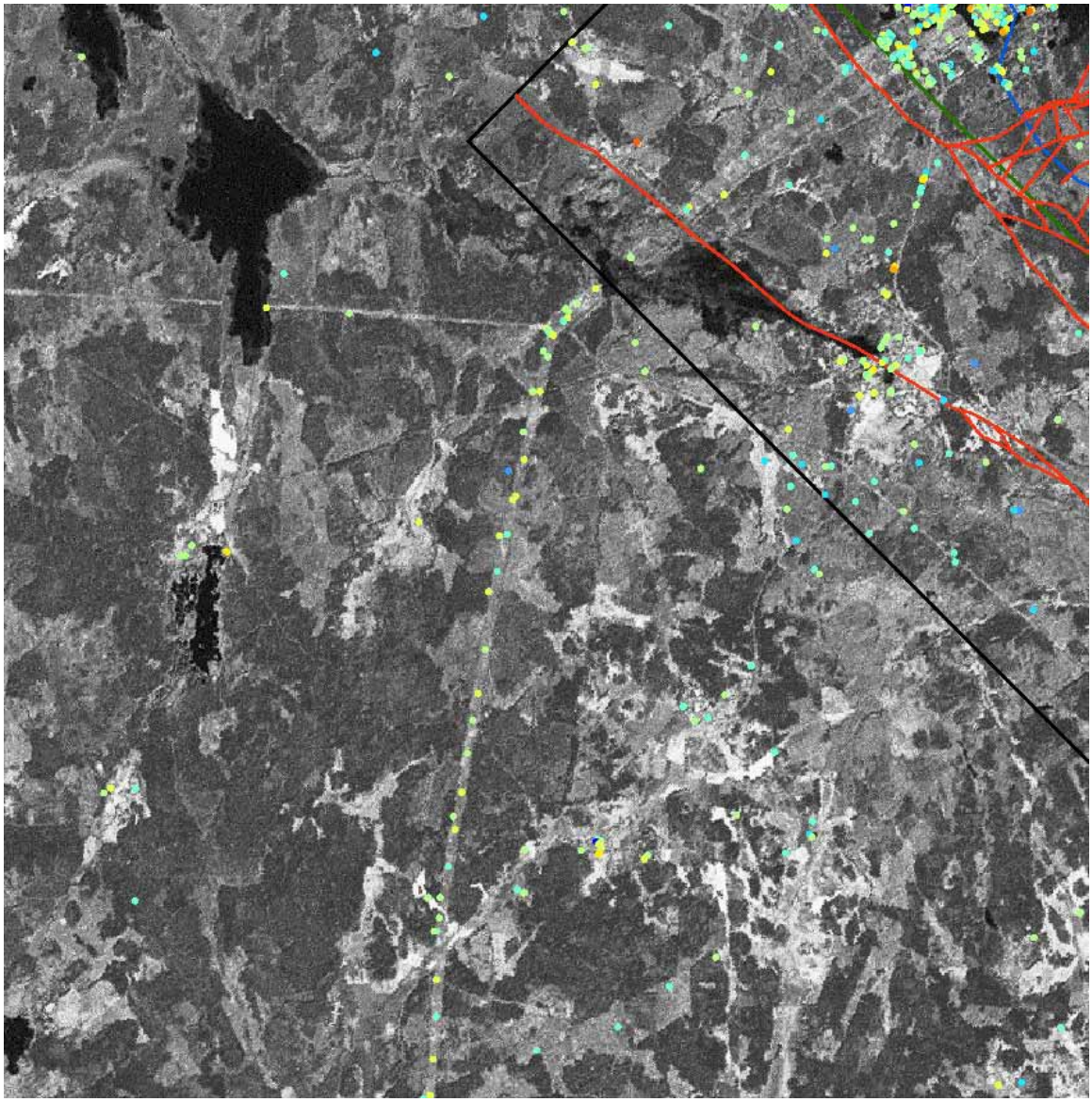

Figure 8. *Extract from Mapsheet 1. Note the number of data points along the power line. Vertical metal structures act as exceptionally good scatterers.*

Figure 9 shows the town of Östhammar. Numerous buildings are undergoing subsidence. They are not spatially correlated, however, suggesting that the subsidence is due to poor foundations and/or collapse of the buildings themselves. This is also the case for a number of buildings in the region. Figure 10, for example, shows a number of subsiding buildings in the rural area east of the model area.

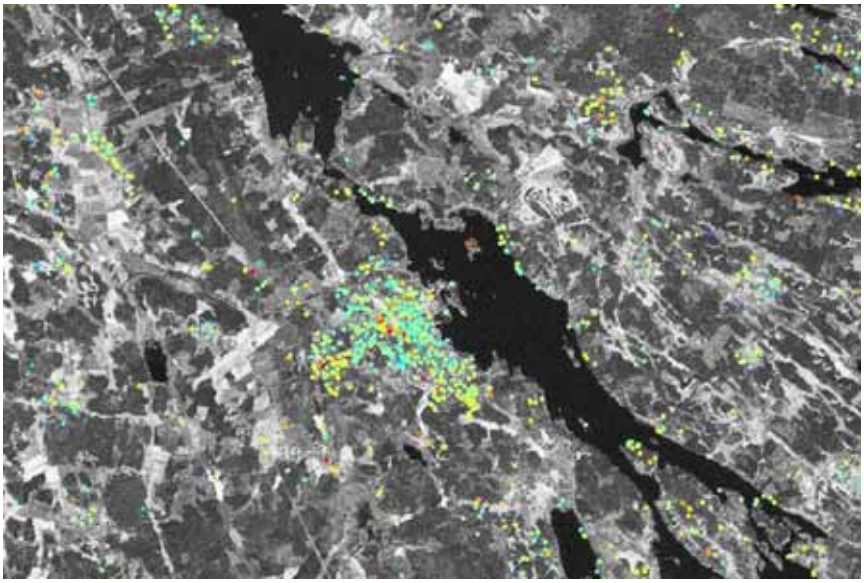

Figure 9. *Town of Östhammars. Numerous buildings are undergoing subsidence.*

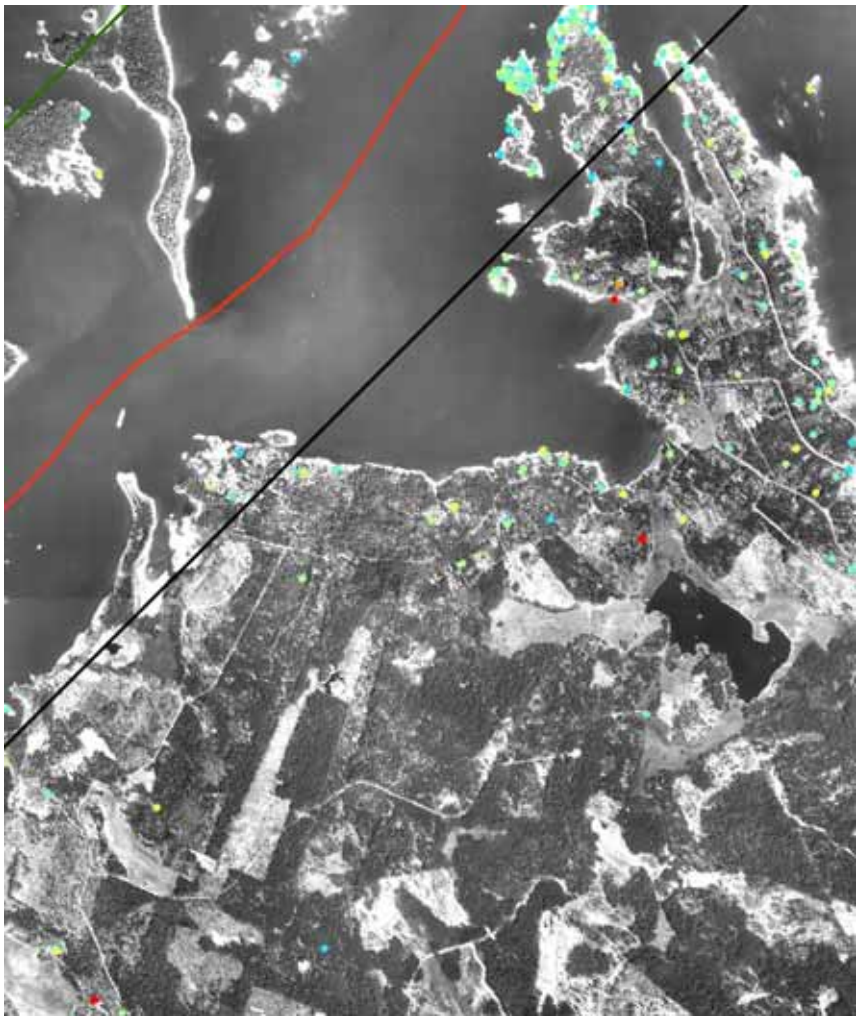

Figure 10. *Rural area just east of the model area. Three buildings in the area show significant subsidence.*

3.2 Problems in determining regional trends

Mapsheet 2 shows all the PS at a scale of 1:50,000. Two main classes of objects act as permanent scatterers in this area. The first are natural reflectors, such as rocks. The second are man-made reflectors, such as parts of buildings. The PS technique determines movement relative to an arbitrarily chosen PS. There are many reasons why one object may be moving relative to the others. An old building may be collapsing. A building may be subsiding due to poor structural foundation. An area of sediments may be undergoing compaction due to loading, or due to lowering of pore pressure due to groundwater extraction. Regional causes may include crustal tilting due to isostatic uplift, or active tectonics. In addition, there are sources of error such as inaccuracy of satellite orbital information.

One of the most difficult challenges faced in this type of study is to distinguish and quantify the different contributions to the velocities measured. Indeed, there are no established quantitative techniques that can separate regional displacements, local displacements and point displacements. Linear interpolators, such as kriging, assume no regional trend. Deterministic spatial interpolators, such as inverse distance, are highly affected by the strong spatial clustering typical of these data.

Since the object of this investigation was to determine if any differential movement could be detected across faults in the Forsmark area, the dataset was divided into three groups for analysis. The division was based upon the location of regional lineaments provided by SKB (Figure 11). Both statistical and geostatistical techniques were used.

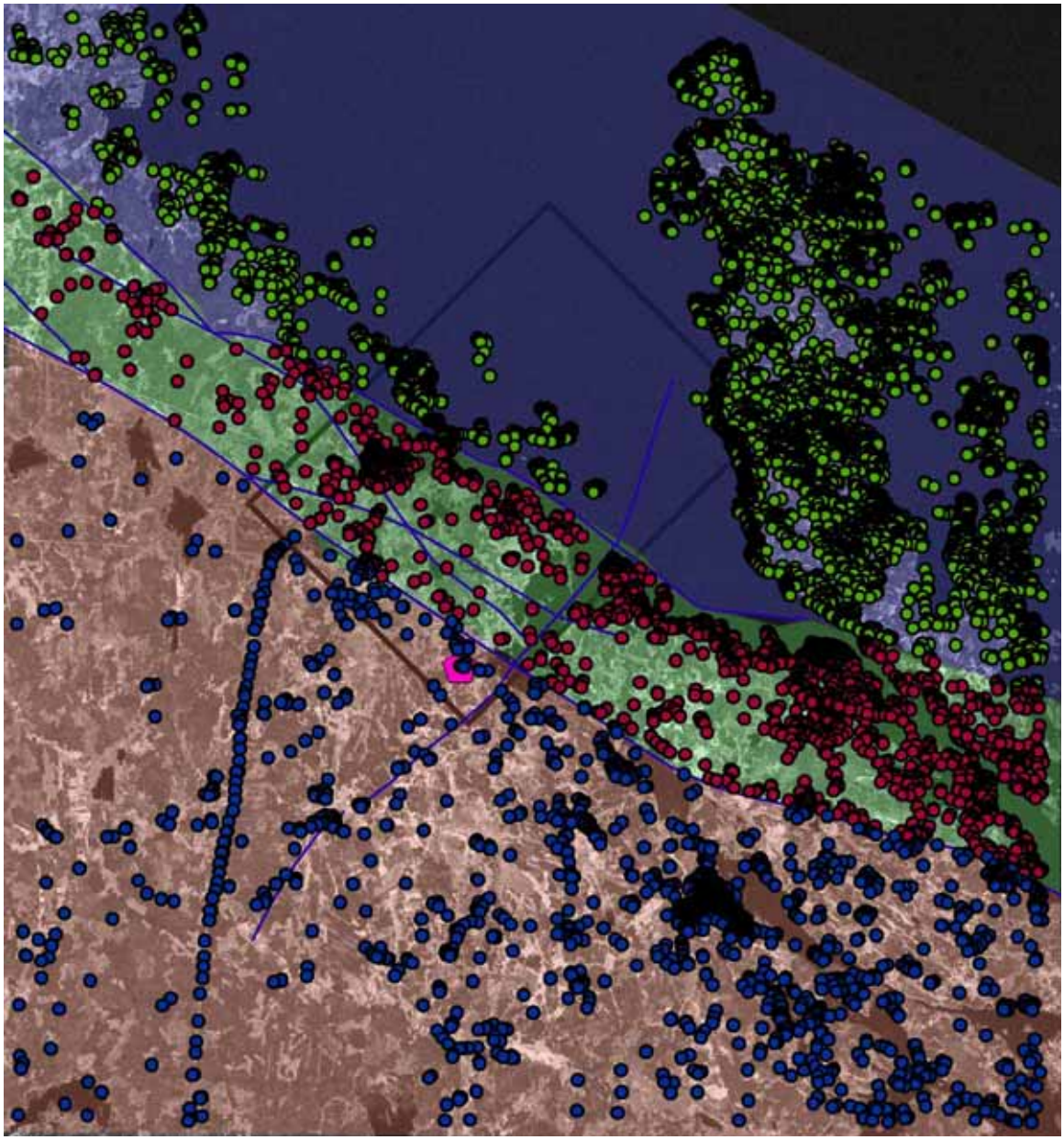

Figure 11. *Division of PS into three groups, based upon blocks defined by regional lineaments.*

3.3 Statistical comparison of populations

Figure 12 shows the distribution of velocities for the entire population. Figure 13 shows the comparison of means, medians, and standard deviations for the three blocks, as well as the entire population. We define Block 1 as the northernmost block, Block 2 as the central block and Block 3 as the southernmost block. Block 1 has a significantly higher number of scatterers because it includes most of the coastline.

All of the frequency distributions have very long tails, with more outliers on the negative side than the positive side. This is expected, as we expect most of the scatterers to be fairly stable. Those with significant movement are more likely to be undergoing subsidence than uplift.

Since we are not interested in outliers, who represent very local trends, the median is a good estimate of the average velocity. The median velocity for Block 2 is zero. The median velocity for the northern block is 0.1 mm/yr, implying uplift relative to the centre block. The median velocity for the southernmost block is –0.1 mm/yr, implying subsidence relative to the centre block. The difference is too small to be conclusive without looking at the spatial distribution of the velocities within each block.

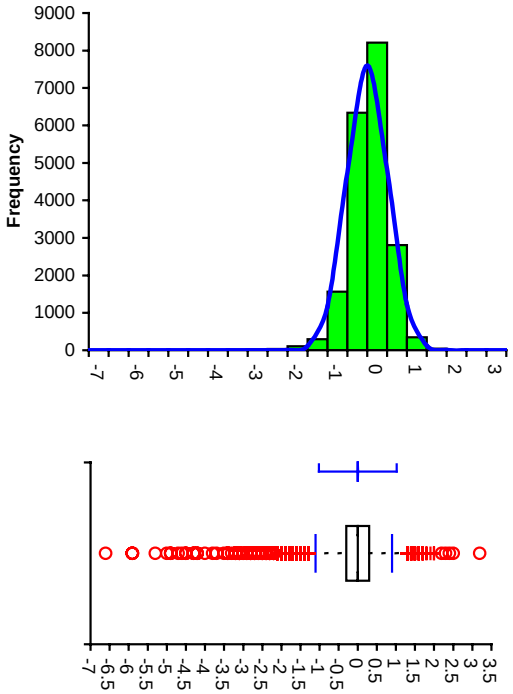

n	19811
Mean	0.005
95% CI	-0.002 to 0.012
Variance	0.2703
SD	0.5199
SE	0.0037
CV	9981%
Median	0.000
95.0% CI	0.000 to 0
Range	9.80
IQR	0.60

Percentile	
2.5th	-1.100
25th	-0.300
50th	0.000
75th	0.300
97.5th	0.900

Figure 12. *Frequency distribution and summary statistics for all the PS in the study. The distribution is characterised by long tails, especially on the negative side. The mean and median are both effectively zero.*

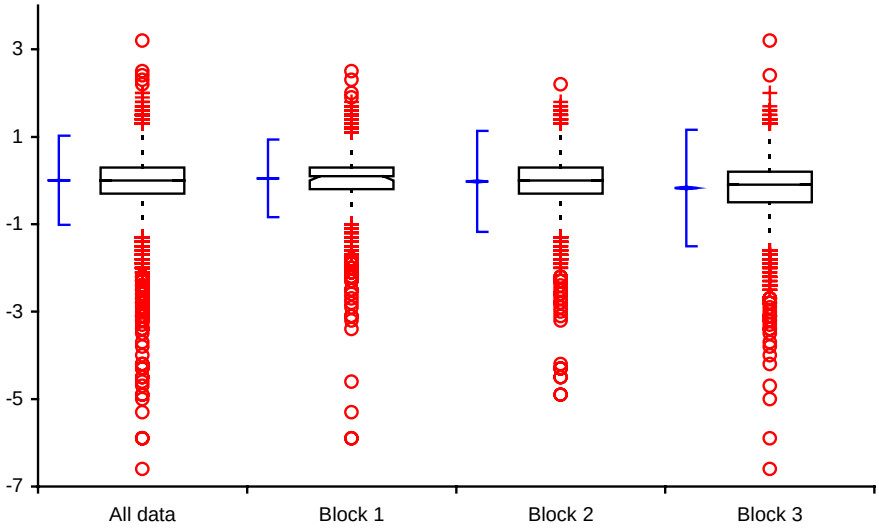

	n	Mean	SD	SE	95% CI of Mean
All data	19811	0.005	0.5199	0.0037	-0.002 to 0.012
Block 1	13683	0.047	0.4522	0.0039	0.040 to 0.055
Block 2	3378	-0.022	0.5883	0.0101	-0.042 to -0.003
Block 3	2785	-0.171	0.6799	0.0129	-0.197 to -0.146

	n	Median	IQR	95% CI of Median
All data	19811	0.000	0.600	0.000 to 0
Block 1	13683	0.100	0.500	0.000 to 0.100
Block 2	3378	0.000	0.600	0.000 to 0
Block 3	2785	-0.100	0.700	-0.100 to -0.100

Figure 13. *Comparative statistics for the three blocks. The difference between the highest and lowest median velocity is 0.2 mm/yr. The difference between the means is similar.*

3.4 Spatial comparison of populations

The difficulties in quantifying regional trends in this type of data are illustrated in Figure 14. In this map, a local polynomial estimate was done over each block separately. The results are highly biased by local trends and missing data. Apparent differences across the block boundaries cannot be considered significant.

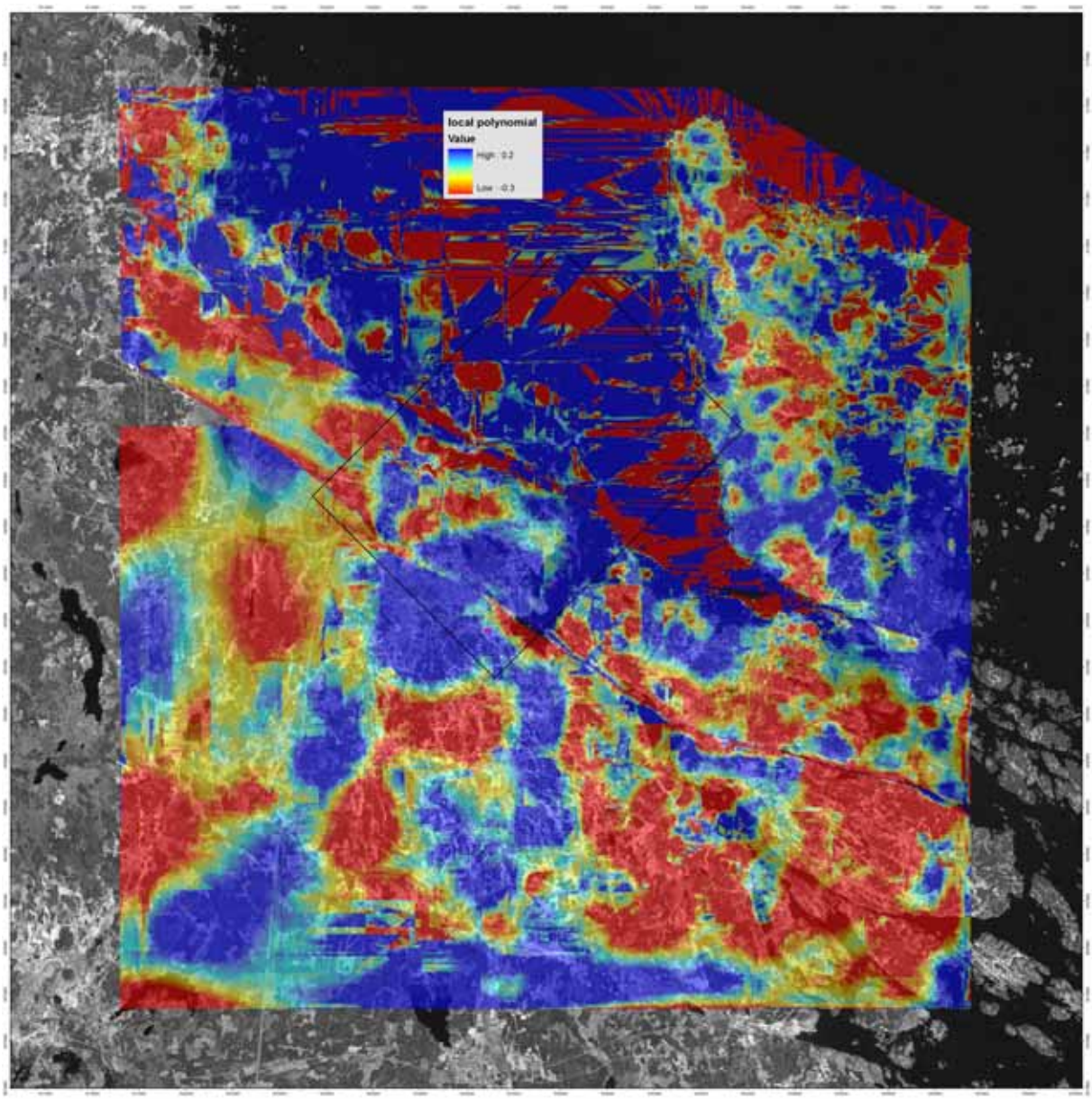

Figure 14. *Local polynomial gridding of the PS data, with each block gridded separately. The results are highly affected by spatial clustering of the data and local movements.*

Various other gridding techniques, including kriging, were tested. All were excluded except fitting of a first order polynomial (a plane). This is shown in Figure 15. Although the blocks appear to be tilting, the magnitude is very small, and cannot be considered significant, given the possible errors involved in the calculations.

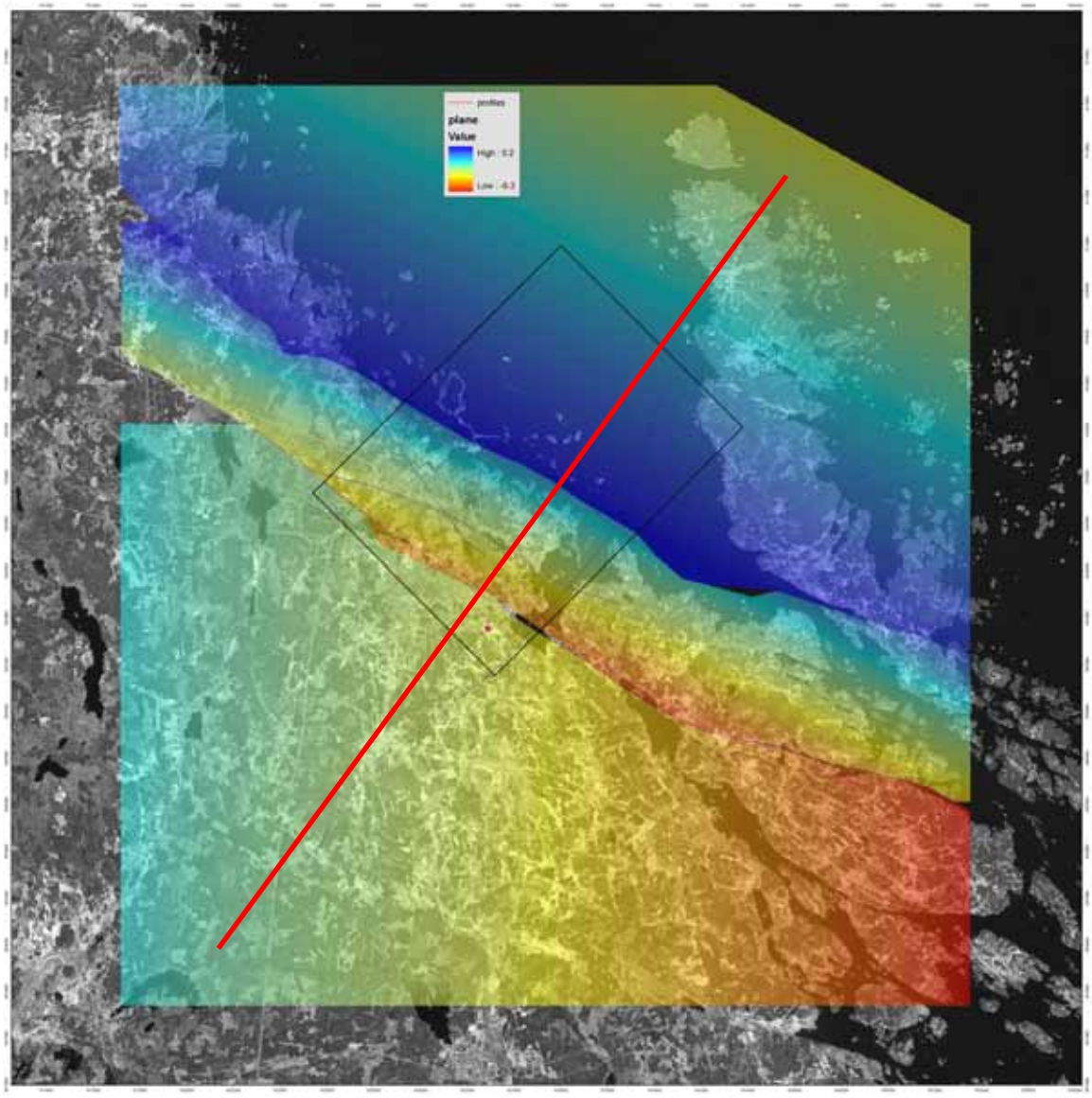

Figure 15. *Regional trends of velocities in the three blocks were determined by fitting a first order polynomial to the data. The red line shows the location of the profile shown in Figure 16.*

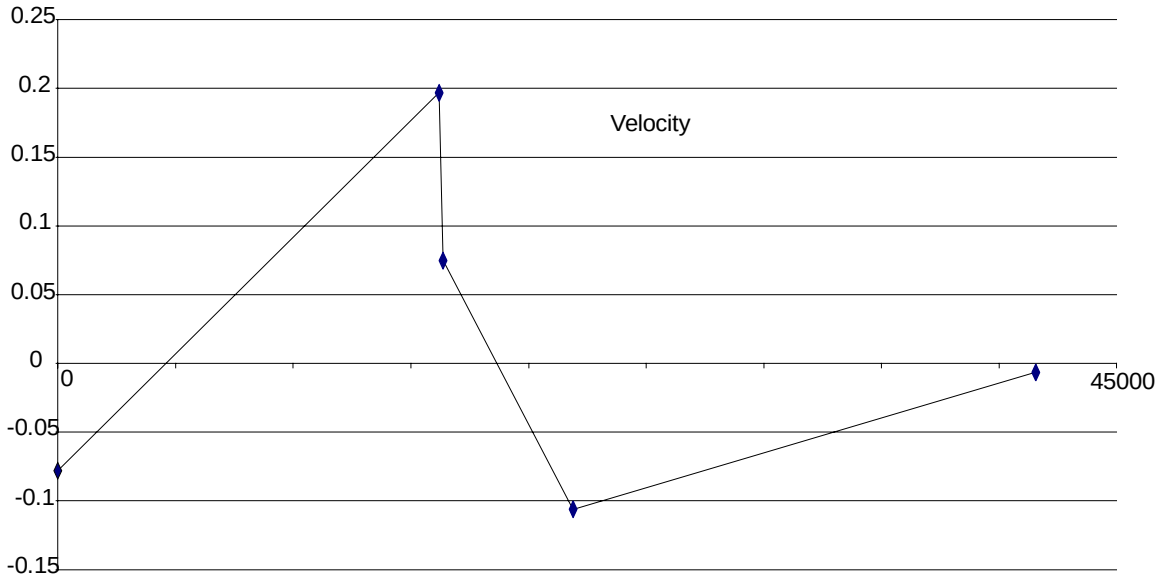

Figure 16. *Profile of regional velocity trends shown in Figure 15. The profile runs from northeast to southwest. The magnitude of the apparent tilting is much smaller than the possible error level.*

4. Conclusions

In this study we have succeeded in identifying almost 20,000 stable reflectors, either natural or manmade. Satellite to ground line-of-site velocity has been determined for each of these reflectors, with precision better than 1 mm/yr. Many local subsidence phenomena have been identified, for example compaction in loose sediments. Analysis of movement trends across regional lineaments does not support the hypothesis of slow, aseismic vertical movement taking place along these features. Horizontal movement cannot be ruled out.

For future monitoring applications, it would be useful to install artificial reflectors in well-chosen locations. NGU has installed six such reflectors in two locations in Norway (Figure 17). The reflectors are relatively inexpensive to build (approximately NOK 30,000) and can act as a supplement to GPS and other measuring techniques. By installing them on bedrock, it can be assured that any movements measured are not due to compaction or other local phenomena.

With the failure of gyroscope 1 onboard ERS-2 on January 7, 2001, very few images have been of sufficient quality to use for interferometry. The ESA satellite ENVISAT, launched in March, 2002, is in the same orbit as ERS-2 and able to obtain very similar images using it's ASAR instrument. It is possible to combine ERS and ASAR images to do PS analysis (Colesanti et al., 2003). Another possible source of radar images is the Canadian Radarsat 1 and Radarsat 2 satellites. Unfortunately, all of these satellites only acquire images upon request. It would be advantageous if SKB arranged for the acquisition of both ENVISAT and Radarsat images over possible monitoring sites on a regular basis.

Figure 17. *Artificial corner reflector installed near Tafjord, in Norway. The reflector is constructed of 10mm thick aluminum.*

5. References

Colesanti, C., Ferretti, A., Prati, C., and Rocca, F., **2003**. ERS-ENVISAT permanent scatterers interferometry, Geoscience and Remote Sensing Symposium, 2003. IGARSS '03. IEEE Proceedings, Volume 2: Toulouse, p. 1130-1132.

Dehls, J.F., Olesen, O., Olsen, L., and Blikra, L.H., **2000**. Neotectonic faulting in northern Norway; the Stuoragurra and Nordmannvikdalen postglacial faults: Quaternary Science Reviews, v. 19, p. 1447-1460.

Ferretti, A., Prati, C., and Rocca, F., **2001**. Permanent scatterers in SAR interferometry: IEEE Transactions on Geoscience and Remote Sensing, v. 39, p. 8-20.

Fjeldskaar, W., Lindholm, C., Dehls, J.F., and Fjeldskaar, I., **2000**. Postglacial uplift, neotectonics and seismicity in Fennoscandia: Quaternary Science Reviews, v. 19, p. 1413-1422.

Hicks, E., Bungum, H., and Lindholm, C., **2000**. Seismic activity, inferred crustal strains and seismotectonics in the Rana region, northern Norway: Quaternary Science Reviews, v. 19, p. 1423-1436.

Isaksson, H., Thunehed, H., and Keisu, M., **2004**. Interpretation of airborne geophysics and integration with topography, Stage 1 (2002), P-04-29, Svensk Kärnbränslehantering AB.

Lagerbäck, R., Sundh, M., Svedlund, J.-O., and Johansson, H., **2005**. Forsmark site investigation: Searching for evidence of late- or postglacial faulting in the Forsmark region, results from 2002-2004, R-05-51, Svensk Kärnbränslehantering AB.

Massonnett, D., Rossi, M., Carmona, C., Adragna, F., Peltzer, G., Feigl, K., and Rabaute, T., **1993**. The displacement field of the Landers earthquake mapped by radar interferometry: Nature, v. 364, p. 138-142.

Muir Wood, R., **1989a**. Extraordinary deglaciation reverse faulting in northern Fennoscandia, *in* Gregersen, S., and Basham, P.W., eds., Earthquakes at North-Atlantic passive margins: neotectonics and postglacial rebound: Dordrecht, The Netherlands, Kluwer Academic Publishers, p. 141-173.

—, **1989b**. The Scandinavian Earthquakes of 22 December 1759 and 31 August 1819: Disasters, v. 12, p. 223-236.

Olsen, L., **2000**. Quaternary geology and trenching of the Båsmoen fault, *in* Dehls, J.F., and Olesen, O., eds., Neotectonics in Norway, Annual Technical Report 1999, Volume 2000.001: NGU Report: Trondheim, Geological Survey of Norway, p. 43-46.

SKB, **2004**. Preliminary site description Forsmark area - version 1.1, R-04-15, Svensk Kärnbränslehantering AB.

Appendix: Previous InSAR studies in Norway

Introduction

In 2001, NGU began testing the usefulness of PSInSAR for geological applications in Norway. At that time there had been numerous studies published using the technique in urban setting, mostly in southern climates. One question to be answered was what effect excluding winter scenes would have. Snow covered scenes have completely different reflectivity than 'dry' scenes. Excluding them would not only reduce the available number of scenes to process, but also add a degree of temporal clustering to the data series. The other question to be answered was how many natural reflectors would be identified. The first test area chosen was Ranafjorden, in northern Norway.

Although Norway is situated along a passive continental margin, it is subject to tectonic stresses due to the presence of the Mid-Atlantic Ridge to the north and west. In addition, the Fennoscandian Shield is still experiencing isostatic uplift in response to the melting of the last ice sheets (Dehls et al., 2000). This postglacial uplift is as high as 9 mm/yr in the Gulf of Bothnia, and is responsible for considerable flexural stress along the Norwegian coast (Fjeldskaar et al., 2000). Because of these two forces, there are several large faults that have been active after deglaciation, and may still be active today (e.g. (Dehls et al., 2000; Muir Wood, 1989a)).

Ranafjord is an area with anomalous seismic activity (Hicks et al., 2000). Indeed, it was the location of the largest earthquake recorded in Scandinavia in historical times (Muir Wood, 1989b). The Båsmoen Fault, which runs through the area, was probably active after deglaciation (Olsen, 2000). In addition, due to the steep local topography, the Ranafjorden area was seen to be a good test area for the detection of landslide-related movements. Landslides are a major hazard in Norway and new techniques aimed at monitoring large areas are a major public priority.

Results from Ranafjorden

The PS density was higher than we originally expected, approximately 75 PS/km^2 (overall average value including sea areas). Despite the absence of man-made structures the PS density reached 250-300 PS/km^2 in particularly favourable areas. A correlation of the PS density with the type of rocky surface (Figure 18 is typical) and the local topography was quite evident. Moreover, as expected, the average PS density increased from east to west (Figure 19). This is due to the increasing incidence angle that makes ground resolution finer, reducing the geometric decorrelation.

Figure 18. *Ranafjord has large areas of barren, highly fractured bedrock, with little vegetation. These areas have a very high density of PS.*

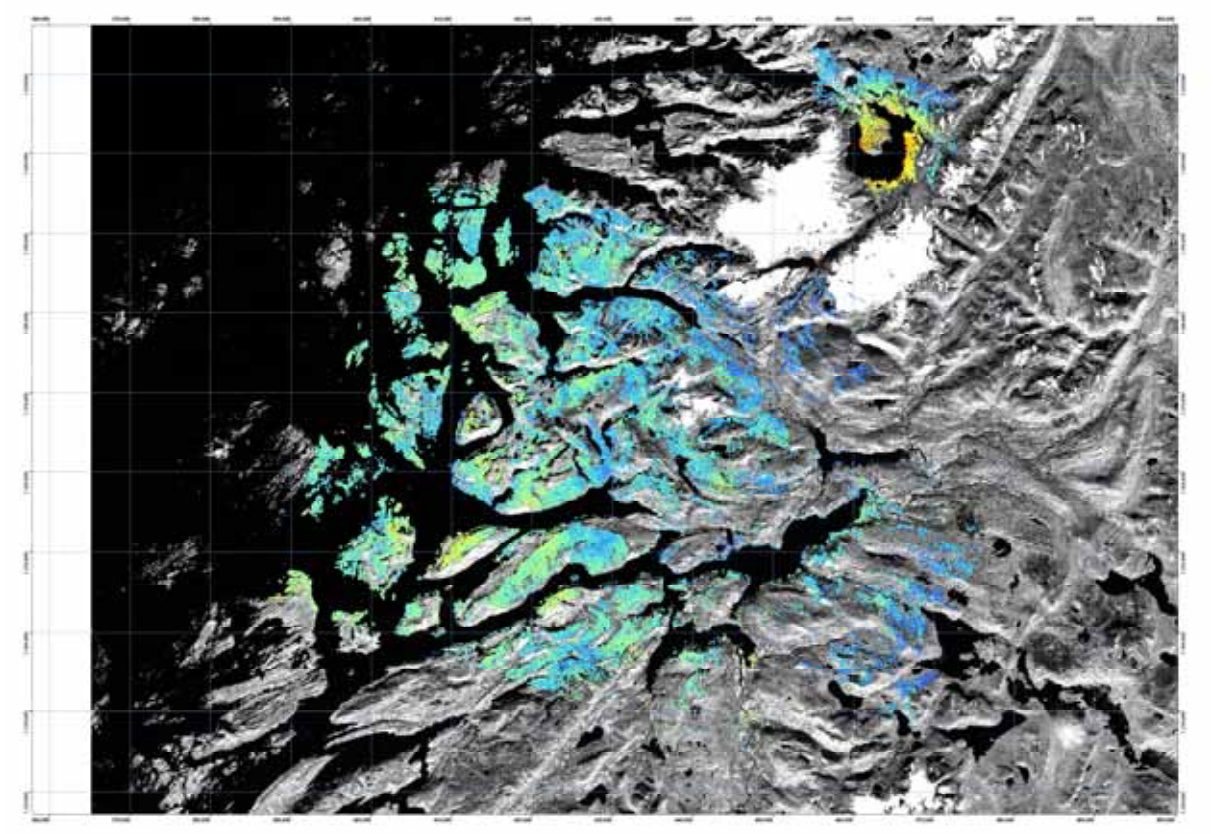

Figure 19. *Average line-of-sight velocity field. PS density increases towards the west due to acquisition geometry.*

The results of the PS analysis show movements at several scales, resulting from various processes, including creep, subsidence and possibly isostatic uplift.

Subsidence/Compaction. Southeast of Mo i Rana is a lake called Storakersvatnet. The northeast outlet of the lake has been dammed as part of a hydroelectric project. Several PS located on the slope of the dam show subsidence rates of up to 8.5 mm/yr (Figure 20). Statkraft, the state power company, has been monitoring compaction in the rock-filled dam since its construction two decades ago. Measurements at the thickest part of the dam show a compaction rate of approximately 18 mm/yr during the period 1992 to 2000. The compaction rate is proportional to the thickness of the dam material, so the lower velocities measured by our analysis is likely due to the placement of the PS on the lower part of the dam.

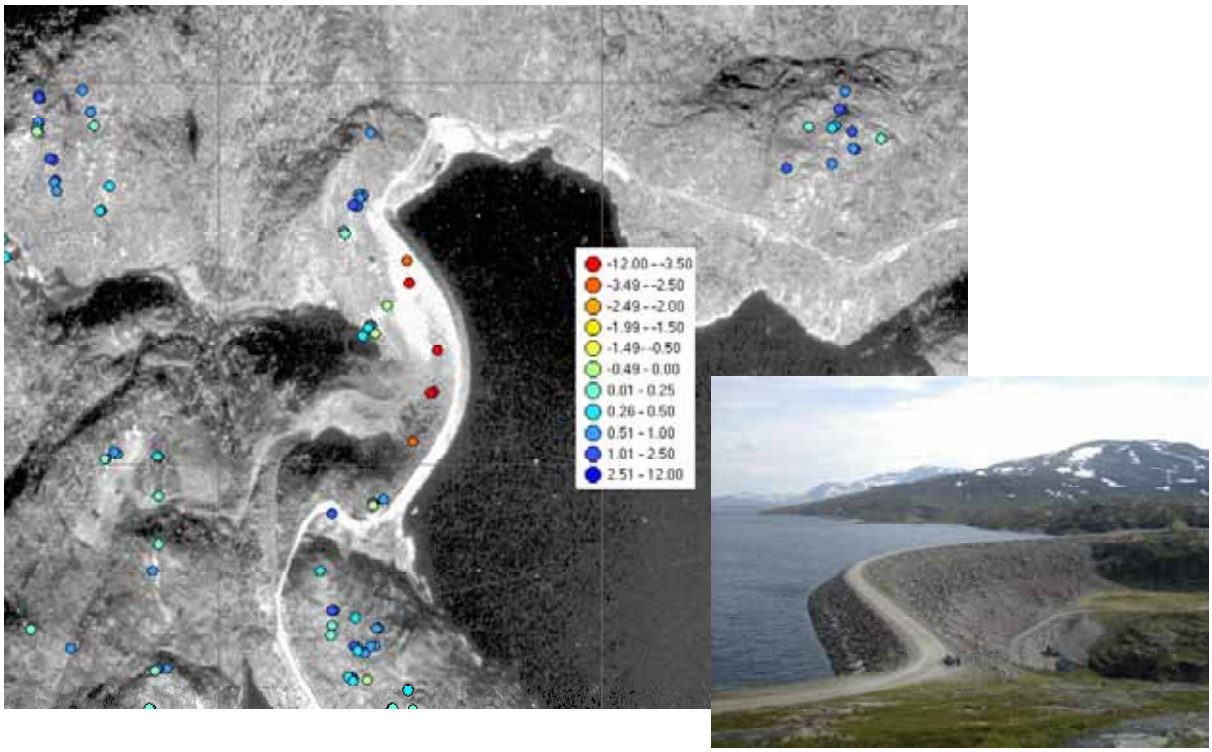

Figure 20. *Compaction in a rock-filled hydropower dam. Some component of creep is probably present as well.*

Creep. Many steep slopes in the Ranafjorden area are covered with blocky colluvium, deposited by rock and snow avalanches. Most of these deposits are stable, but large blocks or portions of the slopes seem to creep down slope due to gravity (Figure 21). Vertical velocities are up to 5 mm/yr. This implies a higher true velocity as there is also a horizontal component to the movement of the deposits.

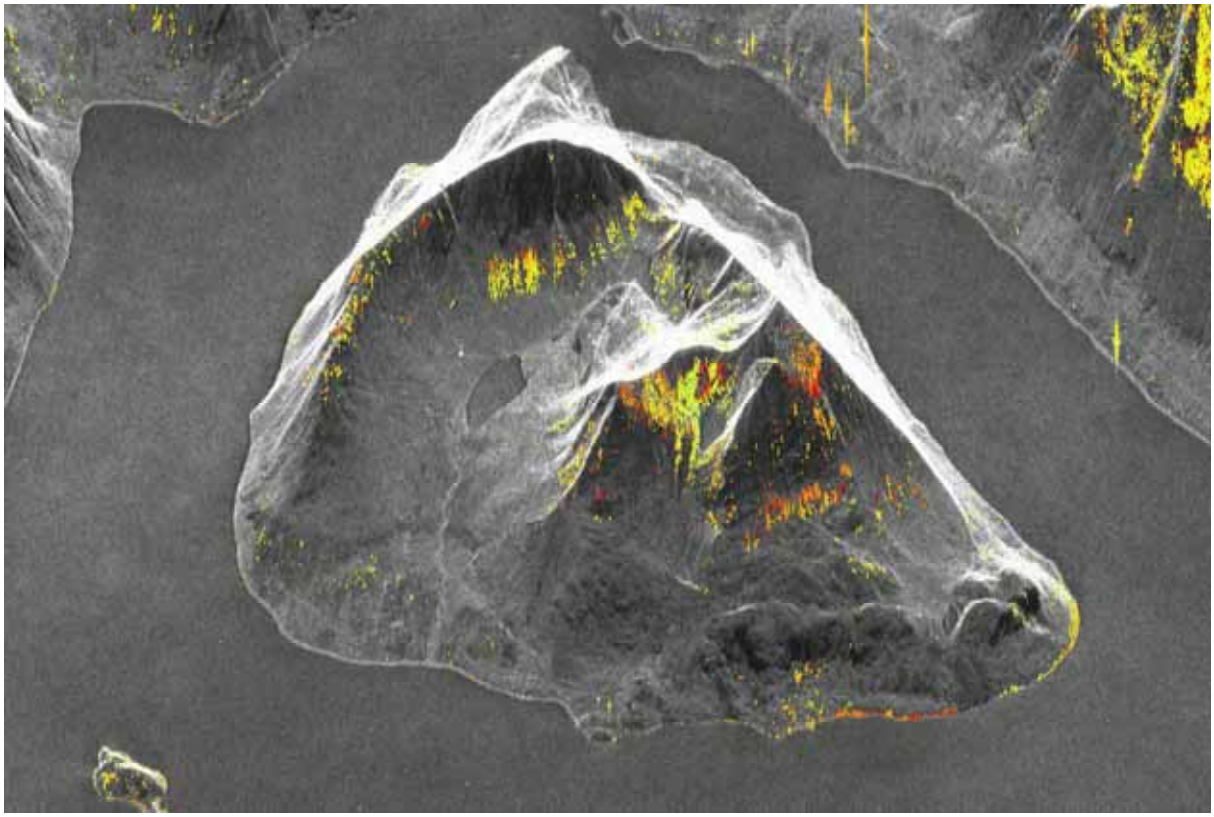

Figure 21. *Slow (3-5 mm/yr) gravitational creep in blocky colluvium. The red points are moving whereas the yellow ones are stable.*

Isostatic uplift. Although there is certainly a component of postglacial isostatic uplift in the velocity field we measure, it is difficult to quantify. PS deformation data are relative to a Ground Control Point (like all interferometric measures). Their accuracy decreases with the distance from the GCP, low spatial frequency components of the velocity field (e.g. low order polynomials) require a careful analysis before being considered reliable. Although the low frequency component visible in the data is compatible with known rates of uplift in the region, it is also within the error range of the technique.

Elastic crustal deformation.

Figure 22 shows the area around Svartisen hydropower reservoir. This reservoir is the second largest in Norway. Between 1997 and 1998, after the construction of new dams, the water level was increased by 100 metres, equivalent to about 3 km^3. This extra load resulted in about 4 cm of depression in the gneissic bedrock, due to elastic deformation.

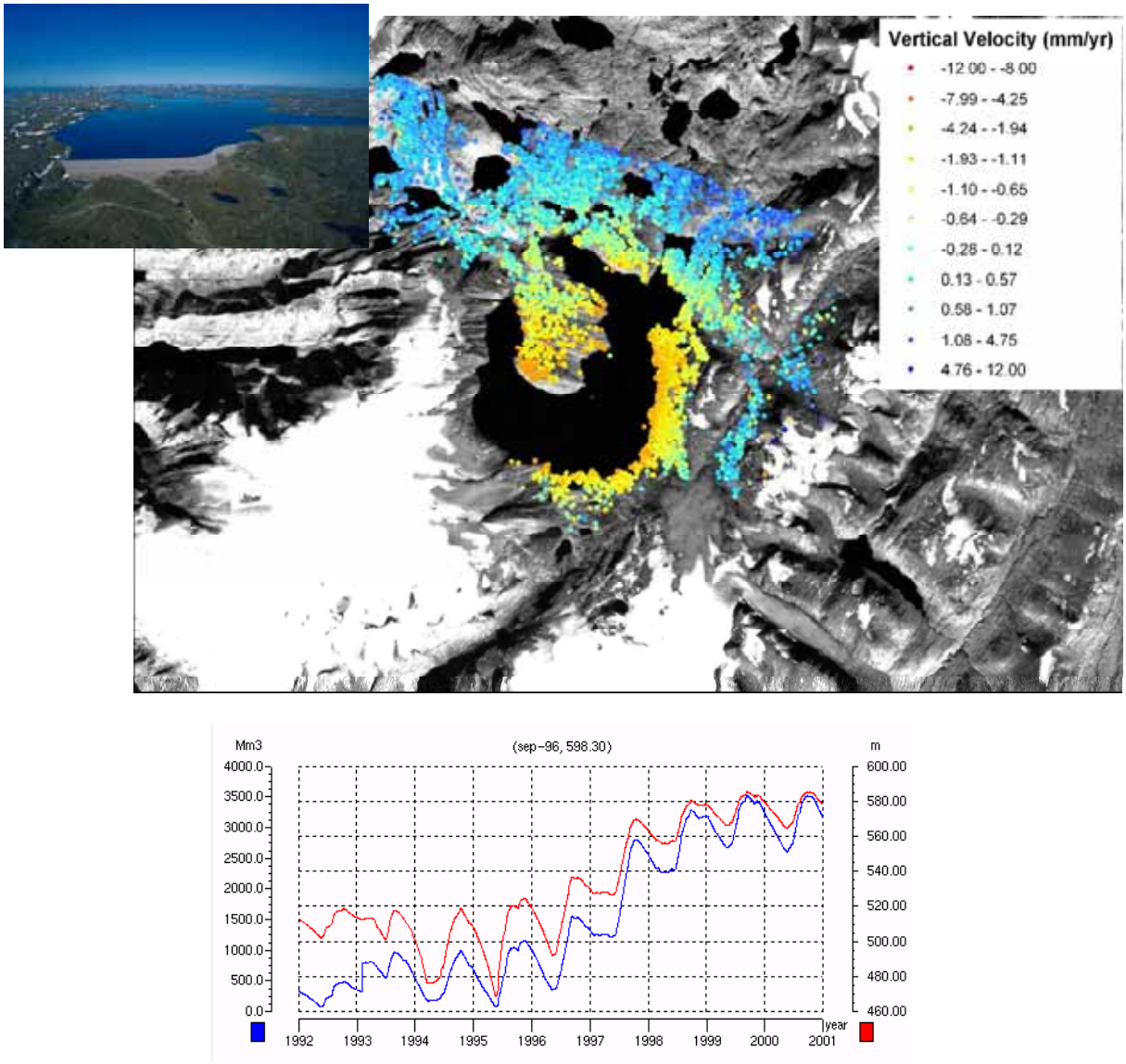

Figure 22. *Svartisen hydropower reservoir. Increase of water level by 100 metres between 1997 and 1998 led to 4 cm of depression in the gneissic bedrock.*

Tectonic deformation. At this time is in not possible to distinguish a tectonic component in the velocity field. Further analysis must be done to separate the velocity field into various spatial frequency components. Once local creep and compaction phenomena are separated from the signal, and low wavelength phenomena such as isostatic uplift identified, the remaining velocity field can be examined to identify tectonic deformation.

PSInSAR in an urban setting: Oslo and tunnel construction

NGU has also studied interferometry results for both Trondheim and Oslo. In an urban setting, the density of PS is very high, often over 1000 PS/km^2. Results have corresponded very well with *a priori* information such as historical levelling data. In Oslo, one particular area was of special interest to us.

Involvement in the project "Tunnels for citizens" led us to speculate that perhaps this technique could be useful in identifying and quantifying short-term subsidence due to underground construction. The well-known subsidence caused by groundwater drainage

during the construction of the Romeriksporten tunnel presents a perfect test case. Levelling had been done on a number of buildings before, during and after construction.

Advanced processing was carried out using 48 images from track 337, covering the time period 1992 to 2002. The area processed covered the western part of Romeriksporten tunnel, as well as the Alnabru area to the north. The area processed included the areas most affected by the groundwater withdrawal associated with tunnel construction.

In order to identify subsidence related to the tunnelling activity, displacement-time series were generated for all points, including those with low coherence. These charts were then examined to identify non-linear displacement. Numerous houses showed accelerated subsidence during the time of tunnelling. Indeed, subsidence in Godlia clearly began before subsidence in Hellerud (Figure 23), as expected from the progress of the tunnelling. In other cases, ongoing subsidence showed no acceleration during the time of tunneling, suggesting that the subsidence was unrelated to construction.

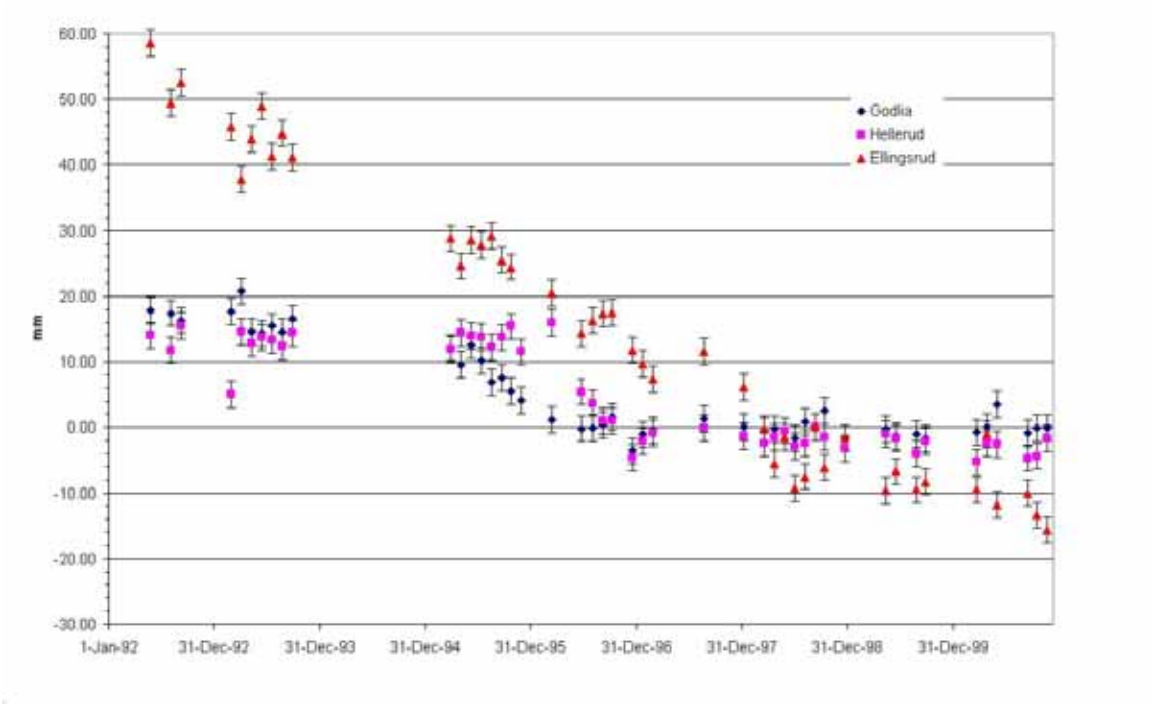

Figure 23. *Displacement-time series for selected houses along the trace of the Romeriksporten tunnel. Accelerated subsidence in Hellerud and Godlia coincides with the time of tunnel construction in those areas. The subsidence in Ellingsrud shows no acceleration, as is unrelated to tunnel construction.*

Comparison with levelling. Jernbaneverket had a program for monitoring subsidence related to the construction of Romeriksporten tunnel. Many buildings were levelled before, during and after tunnel construction. Others were levelled only after subsidence was detected. We were supplied with the levelling data from a number of houses in Hellerud, Godlia and Ellingsrud in order to evaluate the results of the PS technique.

In the Figures 24 to 27, displacement-time series from permanent scatterers have been shown, even if they have low coherence. Since the signal-to-noise ratio for these points is quite low, individual displacements between successive images cannot be measured accurately. Nonetheless, the general trends show clear offsets that compare well with independent observations.

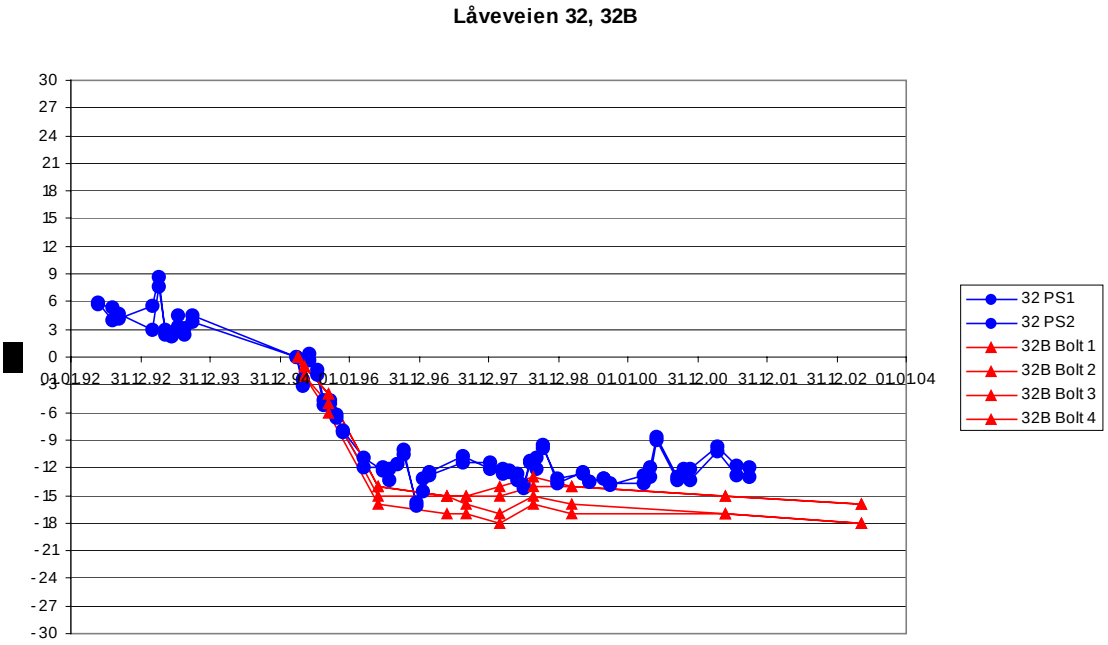

Figure 24. *Subsidence measured in Låveveien 32B by levelling compared with PS from Låveveien 32, next door. PS velocity is along the line of sight with the satellite (23º from vertical). Blue dots are from PS. Red triangles are from bolts on the corners of the house.*

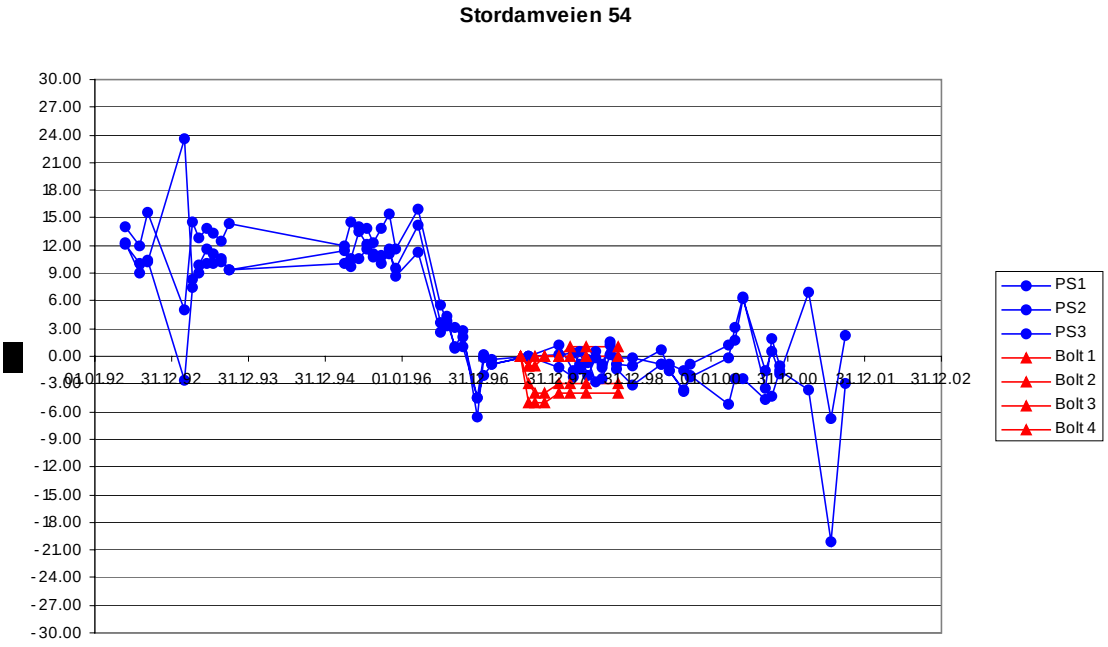

Figure 25. *Subsidence measured in Stordamveien 54 by levelling compared with three PS from the same building. Although the signal-to-noise ratio is low, PS measurements reveal subsidence not detected by levelling, which began only afterwards. Blue dots are from PS. Red triangles are from bolts on the corners of the house.*

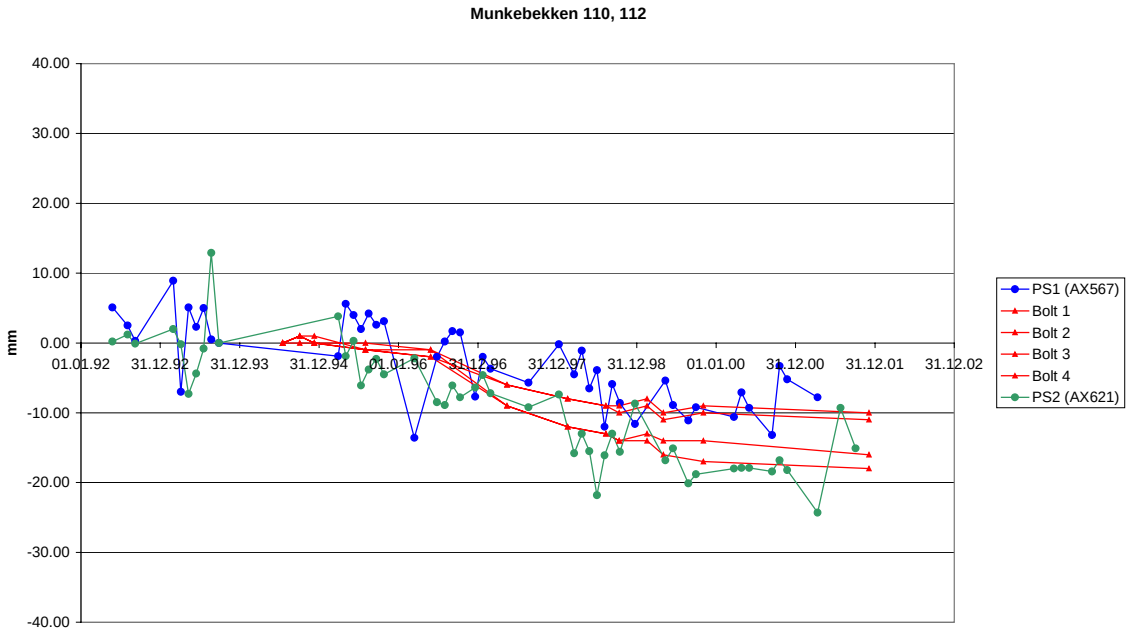

Figure 26. *Despite a low signal-to-noise ratio, the PS measurements agree well with those obtained by levelling. Note that the levelling results show not only subsidence, but tilting of the building.*

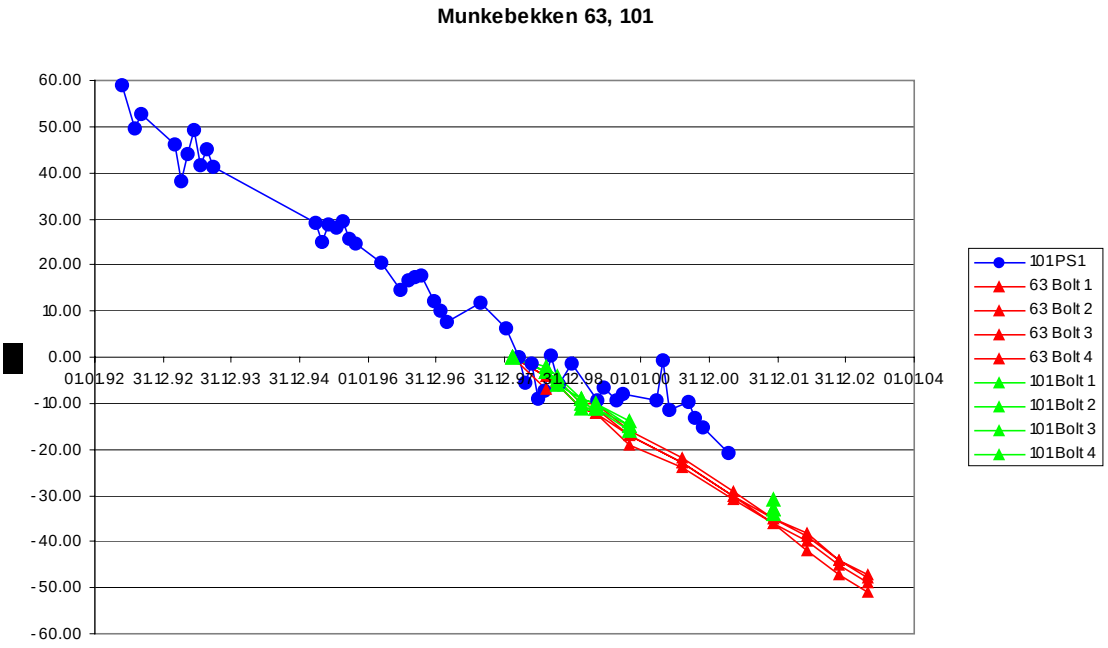

Figure 27. *Levelling at both Munkebekken 63 and Munkebekken 101 shows a steady rate of subsidence from 1997. PS analysis shows that this subsidence has had a nearly constant rate since 1992 and cannot be related to the tunnelling activity. Blue dots are from PS. Red triangles are from bolts on the corners of the house.*

Summary. By using the archive of ERS scenes available from 1992 to 2001, we have been able to compare and contrast the results with those obtained by other techniques. We were able to detect subsidence and construct displacement-time series for numerous buildings that experienced up to 2 cm displacement over the period of tunnel construction. Buildings that experienced higher rates of subsidence were not detected due to unwrapping errors.

Although we were not able to detect and measure subsidence in all buildings, where measurements were obtained, they are in close agreement with those obtained from optical levelling. More importantly, perhaps, we were able to identify and measure displacement in a number of buildings that had not been monitored by other techniques.